Research article

Metabolomics study of graphene nuangong acupoint plaster for primary dysmenorrhea

Wu Liu [a], Ting Zhang [b], Zhaoduan Hu [a], Xin Li [a], Fuchun Wang [c,*], Rui Peng [a,**]

[a] College of Acupuncture and Orthopedics, Hubei University of Chinese Medicine, Wuhan, 430065, China
[b] Department of Rehabilitation Medicine at Jingzhou Central Hospital, Jingzhou, 434020, China
[c] Department of Acupuncture, The Affiliated Hospital of Changchun University of Chinese Medicine, Changchun, 130117, China

ARTICLE INFO

ABSTRACT

Primary dysmenorrhea is a common gynecological disease with typical clinical symptoms and diverse treatment methods. Acupoint patch therapy is one of the traditional external treatments of traditional Chinese medicine, with a long history, and has been widely used in the treatment of many diseases in China. Graphene nuangong acupoint plaster (GNGAP) developed based on traditional acupoints and new materials have been used in the clinical treatment of primary dysmenorrhea, and satisfactory therapeutic effects have been achieved. However, the underlying mechanisms of GNGAP still need further investigation. In this study, we used estradiol benzoate combined with oxytocin intraperitoneally to establish dysmenorrhea model rats, and observed the torsion response, uterine organ coefficients, prostaglandin levels and metabolite changes of rats with dysmenorrhea model after the intervention of GNGAP, to elucidate the mechanism of the effect of GNGAP. Compared with normal rats, the dysmenorrhea model rats exhibited increased writhing response and latency time, increased uterine organ coefficient, and significant changes in 79 metabolites. Twenty-three significantly enriched pathways were discovered, including amino acid metabolism, arachidonic acid metabolism, pyrimidine metabolism, and ovarian steroidogenesis, which may be involved in the pathogenesis of primary dysmenorrhea. Compared with the model group, the torsion response, latency time and uterine organ coefficient of rats in the acupoint patch group were significantly improved, and nine uterine metabolites were significantly altered, among which metabolites such as 4-pyridoxic acid, D-glucarate and Phenol were identified as potential biomarkers for the therapeutic effects of GNGAP. Vitamin B6 metabolism, Ascorbate and aldarate metabolism and Tyrosine metabolism were enriched in nine metabolic pathways. These findings contribute to the screening study of potential pathological metabolic pathways in primary dysmenorrhea. Additionally, they reveal the biological effects of GNGAP in the treatment of primary dysmenorrhea at the metabolite level.

1. Introduction

Primary Dysmenorrhea (PD) is a common gynecological disease characterized by cyclic lower abdominal pain during the menstrual

---

cycle, in the absence of pelvic pathological changes, and it typically occurs within 6–24 months after menarche, with an incidence rate of 50 %–90 % among females [1]. The clinical symptoms of this disease have certain characteristic features, and the main symptom experienced by patients is lower abdominal pain, which may radiate to the lower back and inner thighs. The pain is often spasmodic and intermittent, with regular occurrence during menstruation. The nature of the pain is similar in each episode. Patients may also experience discomfort such as nausea, vomiting, diarrhea, and headache, the severity of which can affect the sleep and quality of life [2]. First-line medical treatments for PD include nonsteroidal anti-inflammatory drugs (NSAIDs) and hormones, both of which can alleviate the clinical symptoms of PD by inhibiting the production of prostaglandins in the uterus, but they may also cause adverse reactions, such as NSAIDs may lead to gastrointestinal discomfort in patients, while hormone medications may disrupt menstrual patterns and even affect fertility [3]. In addition, surgical interventions, vasodilators, calcium channel blockers, Chinese herbs, acupuncture, and transcutaneous electrical nerve stimulation (TENS) have shown certain clinical efficacy, but due to limitations in the quality of clinical evidence, further validation of the effectiveness of some of these therapies is still required [4].

In recent years, there has been an increasing amount of research on the treatment of PD using both traditional Chinese medicine (TCM) and Western medicine. And significant progress has been made in understanding the pathogenesis and therapeutic approaches of this disease [5,6]. Acupoint application therapy is one of the traditional external treatments in TCM, which is not only has a simple application method and no significant side effects but also reduces psychological stress during treatment, making it well accepted among patients. Researchers found through network meta-analysis that acupoint application therapy has certain advantages in clinical efficacy and symptom improvement for PD [7]. However, traditional acupoint application therapy has limitations regarding the onset time, allergic reactions, drug penetration, and prescription formulation, which hinder its clinical promotion. To address these limitations, the research team has upgraded the materials and improved the techniques used in acupoint application products. We have incorporated water-soluble high-polymer medicinal adjuvants and graphene powder as carriers, utilizing their water solubility and strong molecular adsorption capacity to effectively enhance the dissolution and mutual stabilization of active ingredients in Chinese medicine, thereby improving transdermal drug penetration. Nevertheless, the mechanism of how graphene Nuangong acupoint plaster (GNGAP) treats PD remains unclear. Therefore, in this study, we employed a rat model of PD and applied GNGAP for intervention. We observed the twisting response, uterine organ coefficient, prostaglandin levels in the normal control group, model group, and graphene nuangong acupoint plaster group of rats. Additionally, we analyzed uterine metabolites using non-targeted metabolomics techniques to investigate the analgesic mechanism of GNGAP, providing new research insights into the external treatment methods of TCM.

2. Experimental material

2.1. Laboratory animals and groups

Eighteen female virgin SPF-grade SD rats (7–8 weeks old, weighing 200 ± 20 g) were selected for this study. The rats were purchased from Changchun Yisi Experimental Animal Technology Co., Ltd. (Jilin Province Experimental Animal Quality Certificate No.: 202200042265). All the rats were housed at the Animal Experimental Center of Changchun University of Chinese Medicine. After a 3-day adaptation period, the rats were randomly divided into three groups: normal control group, model group, and graphene nuangong acupoint plaster group, with 6 rats in each group. Roman numerals were used to mark the rats' tails for differentiation after grouping. This animal experimental protocol has been approved by the Ethics Review Committee for Animal Experiments of Changchun University of Chinese Medicine, with approval number: 2022005.

2.2. Main reagents and instruments

Project-specific Graphene Nuangong Acupoint Plaster (1 cm * 1 cm size, Jilin Ailuokang Pharmaceutical Technology Development Co., Dedicated to National Key R&D Program Projects); Estradiol Benzoate Injection (Harbin Sanma Veterinary Pharmaceutical Co., Ltd, Certificate No. (2018) Veterinary Drug GMP Certificate No. 08006, Approval No. (2018) Veterinary Drug GMP Certificate No. 080232511, specification 2 ml: 4 mg); Peptide Injection (Hefei Xinkexin Animal Pharmaceutical Co., Ltd, Certificate No. (2020) Veterinary Drug GMP Certificate No. 12010, Approval No. Veterinary Drug No. 120031571, specification 1 ml); ELISA kits for PGF2α (Wuhan Fabre Biotechnology Co., Ltd, Batch No. E-ELR0795c) and PGE2 (Wuhan Fabre Biotechnology Co., Ltd, Batch No. E-EL-0034c).

Acetonitrile (Brand: Fisher Chemical, Grade: Ultra-pure, High-purity, Content: 99.9 %, Product Specification: 4L, Item No.: A955-4); Ammonium Acetate (Brand: Sigma, Purity: ≥99.0 %, Product Specification: 25 g, Item No.: 73594); Methanol (Brand: Fisher Chemical, Purity: OPTIMA LC/MS, Specification: 4L, Item No.: A456-4); Ammonia (Brand: Fisher Chemical, Grade: Ultra-pure, High-pure, Content: 99.9 %, Product Specification: 2.5LT, Item No.: A470-500).

Mass Spectrometer (AB Triple TOF 6600 Mass Spectrometer, Q Exactive Series Mass Spectrometer); LC Ultra-High Pressure Liquid Chromatograph (Agilent 1290 Infinity LC Ultra-High Pressure Liquid Chromatograph, Vanquish UHPLC Ultra-High Pressure Liquid Chromatograph); Cryogenic High Speed Centrifuge (Eppendorf 5430R); chromatographic column (Waters ACQUITY UPLC BEH Amide, 1.7 μm, 2.1 × 100 mm column).

3. Experimental methods

3.1. Animal modeling

According to the relevant literature [8,9] and preliminary experiments, the project team used a combination of benzoic acid estrogens and oxytocin to prepare a rat model of PD. After an adaptation period of 3 days, except for the normal group, all rats were injected subcutaneously with a combination of benzoic acid estrogens and oxytocin to establish the rat model of primary dysmenorrhea. The inguinal region of the rats was chosen as the subcutaneous injection area. On the 1st and 13th day, benzoic acid estrogens were injected subcutaneously at a volume of 0.5 ml per rat, and from the 2nd to the 12th day, a dosage of 0.2 ml per rat was administered. Twenty-four hours after the last injection of estrogen, each rat was intraperitoneally injected with 2U of oxytocin. During this period, the normal group received an equivalent amount of distilled water injection.

3.2. Methods of intervention

Three groups of rats were subjected to abdominal hair removal prior to the experiment, exposing the entire abdomen. During the experiment, the regrowth of abdominal hair in each group of rats was observed and weighed. If there was regrowth, a second hair removal treatment was performed. The normal group received no intervention other than the aforementioned procedures. The model group underwent modeling without any other interventions. Starting from the fourth day of modeling, the graphene warm uterus acupoint patches group applied acupoint patches on the lower abdomen and lower limbs at the Sanyinjiao acupoint area of the rats. The patches were applied continuously for 5 h once a day for 10 consecutive days. To prevent the patches from falling off, the application sites were secured with medical adhesive tape. To minimize the interference caused by tape fixation, all three groups of rats had the adhesive tape fixed at the same location.

3.3. Evaluation indicators

3.3.1. Twisting frequency

After the administration of the final oxytocin injection, each group of rats was individually placed in an observation cage. The number of twisting reactions and the latency period of twisting within a 30-min period were recorded for each rat. Except for the normal group, the other groups of rats showed an increased number of twisting episodes. The rats primarily exhibited a contracted concave abdomen, torsion of the trunk, extension of the hind limbs, and raised hips. The presence of these behaviors indicated successful modeling.

3.3.2. Coefficient of uterine organs

After the observation of twisting behavior, the rats were anesthetized by intraperitoneal injection for uterine dissection. The personnel involved in specimen collection swiftly extracted fresh uterine tissue on an ice tray. The uterine tissue was then rinsed with homemade pre-chilled PBS buffer to remove blood and any adipose or connective tissues. Afterward, the uterine organ coefficient was measured using an electronic balance. The weighed uterine tissue was sealed in EP tubes and rapidly frozen using liquid nitrogen before being stored at −80 °C in a freezer. The organ coefficient was calculated as the ratio of uterine weight (g) to rat body weight (g), multiplied by 100 %.

3.3.3. Uterine prostaglandin levels

An appropriate amount of frozen uterine tissue was weighed and mixed with 9 times the volume of PBS solution. The mixture was homogenized in a cold grinding machine at 4 °C. After centrifugation at 3000 rpm for 20 min, the supernatant was separated to obtain a 10 % tissue homogenate. Following the instructions provided in the manual, an ELISA assay kit was used to measure the levels of PGE2 and PGF2α in the uterine tissue.

3.3.4. Metabolomics detection

A 200 mg portion of thawed uterine tissue was taken and mixed with a pre-chilled solution of methanol, acetonitrile, and water in a 1:1:1 ratio. The mixture was thoroughly homogenized using a vortex oscillator, followed by 30 min of low-temperature ultrasound treatment and a 10-min incubation at −20 °C. The sample solution was then subjected to centrifugation for 20 min in a low-temperature high-speed centrifuge (speed: 14,000 rpm, temperature: 4 °C). After successful centrifugation, the supernatant was collected and dried under vacuum. For subsequent mass spectrometry analysis, 100 μL of acetonitrile-water solution was added to dissolve the sample, followed by another 15 min of low-temperature high-speed centrifugation. Finally, the supernatant was collected for analysis.

All samples were separated using the Agilent 1290 Infinity LC Ultra-High Performance Liquid Chromatography (UHPLC) system with a HILIC chromatographic column. During the instrumental analysis process, the samples were kept in an automatic sampler at 4 °C. To minimize the impact of instrument detection signals on the results, a random order was used for data analysis of each individual sample. Additionally, during the detection process, quality control (QC) samples prepared earlier were included in the detection sequence to assess the stability and reliability of the detection system and ensure the credibility of the obtained results. After the chromatographic system described above, the researchers used an AB Triple TOF 6600 mass spectrometer to collect the primary and secondary spectra of the samples for mass spectrometry analysis. The detection mode employed was electrospray ionization (ESI)

in both positive and negative ion modes. The secondary mass spectra were collected in data-dependent acquisition (DDA) mode, and the inclusion of spectra was based on peak intensity values. In each scan, up to 10 fragmentation spectra were generated and included for analysis.

3.4. Analysis of experimental data

For the analysis of data related to rat twisting observation, uterine weighing, and prostaglandins, SPSS 26.0 was used to assess differences. Numeric values were presented as mean ± standard deviation (Mean ± SD). One-way analysis of variance (ANOVA) was performed for multiple group comparisons, with P < 0.05 indicating statistical significance.

After chromatography-mass spectrometry analysis, the raw data were converted to .mzXML format using ProteoWizard software. The converted data were then uploaded to XCMS plus software for spectral processing and database searching. Preliminary screening of identified metabolites was conducted based on parameters such as retention time and mass-to-charge ratio. A retention time deviation range of 0.2 min and a mass deviation range of 5 ppm were set. Peak alignment was performed for samples from different groups to ensure the accuracy of identification results. After retention time correction, peak areas of the samples were obtained.

The structures of the identified metabolites were determined using accurate mass matching (<25 ppm) and matching of secondary spectra. Relevant data were retrieved from self-built databases (mzCloud/mzVault/Masslist). The data were preprocessed by Pareto scaling before conducting multidimensional statistical analysis. S-plots and VIP (variable importance in projection) values were obtained after OPLS-DA (orthogonal partial least squares-discriminant analysis) modeling. For univariate analysis, t-tests were used to calculate whether the differences in metabolites between two groups were statistically significant ($P < 0.05$). Additionally, fold change (FC) values representing the magnitude of differences between metabolite groups were calculated, with a threshold of 1.5 for selecting differentially expressed metabolites and a total VIP threshold of 1 for OPLS-DA. The data processing in this study was performed using the Windows 10 operating system, as well as R and Python. After retrieval from databases such as KEGG, HMDB, and LIPIDMaps, differentially expressed metabolites were annotated, and their biological functions and metabolic pathways were analyzed.

4. Findings

4.1. Twisting responses and uterine organ coefficients of each group

The normal control group of rats did not exhibit any twisting responses, and their uterine organs showed no significant swelling. In comparison to the normal control group, the model group of rats had a significantly increased number of twisting episodes ($P < 0.01$) (Fig. 1A), a shortened latency period for twisting ($P < 0.01$)(Fig. 1B), and a significantly increased uterine organ coefficient ($P < 0.01$) (Fig. 1C). In contrast, compared to the model group, the graphene nuangong acupoint plaster group of rats showed a significant decrease in the number of twisting episodes ($P < 0.05$)(Fig. 1A), an extended latency period for twisting ($P < 0.05$)(Fig. 1B), and a significantly reduced uterine organ coefficient ($P < 0.01$) (Fig. 1C).

4.2. Uterine prostaglandin levels

Compared to the normal control group, the model group exhibited a significant increase in $PGF_{2\alpha}$ levels ($P < 0.01$)(Fig. 2A) and a significant decrease in PGE_2 levels ($P < 0.01$)(Fig. 2B)in the uterine tissue. Additionally, the $PGF_{2\alpha}/PGE_2$ ratio was significantly higher in the model group ($P < 0.01$)(Fig. 2C). In comparison to the model group, the graphene nuangong acupoint plaster group showed a significant decrease in $PGF_{2\alpha}$ levels ($P < 0.05$)(Fig. 2A), a significant increase in PGE_2 levels ($P < 0.05$)(Fig. 2B), and a significant decrease in the $PGF_{2\alpha}/PGE_2$ ratio ($P < 0.01$) in the uterine tissue (Fig. 2C).

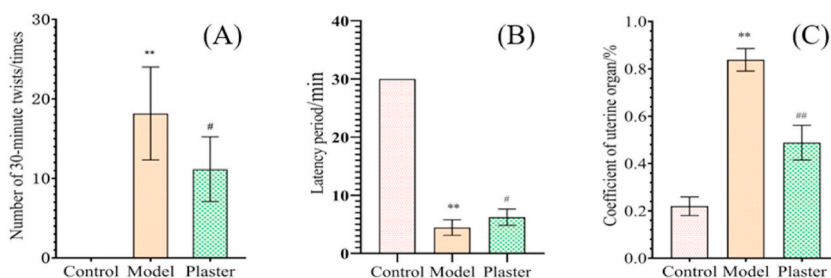**Fig. 1.** Effect of GNGAP on the apparent indexes of PD model rats. Comparison of (A) number of twisting episodes, (B) latency period for twisting, (C) uterine organ coefficient.
Note: Control: Normal control group; Model: Model group; Plaster: Graphene nuangong acupoint plaster group. ** indicates $P < 0.01$ compared to the control group; # indicates $P < 0.05$, ## indicates $P < 0.01$ compared to the model group.
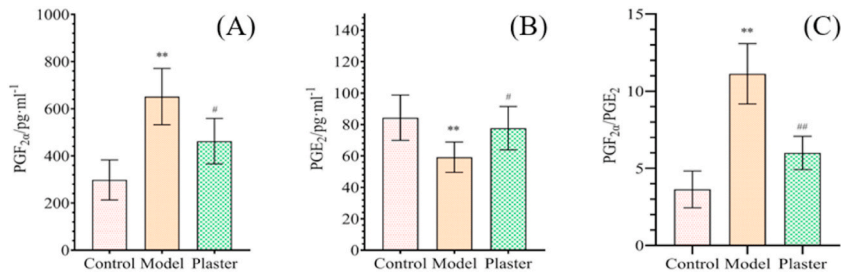
Fig. 2. Effect of GNGAP on the levels of PGF$_{2\alpha}$ and PGE$_2$ in the uterine tissue of PD model rats. Comparison of (A) PGF$_{2\alpha}$ levels, (B) PGE$_2$ levels, (C) PGF$_{2\alpha}$/PGE$_2$ ratio.

4.3. Results of metabolomics analysis

4.3.1. Partial least squares discriminant analysis (PLS-DA)

Further analysis of the metabolic profiles in uterine samples from the normal control group, model group, and graphene nuangong acupoint plaster group was conducted using supervised discriminant analysis, specifically Partial Least Squares Discriminant Analysis (PLS-DA). The PLS-DA scatter plot, shown in Fig. 3, reveals distinct separation between the three groups. To validate the effectiveness of the model, a repeated cross-validation process was performed to obtain model evaluation coefficients. R^2 represents the explanatory power of the model, while Q^2 indicates the predictive ability of the model. A higher Q^2 value closer to 1 indicates better predictive capability of the model. The R^2 value is 0.9674, Q^2 is 0.7307, and Q2 is 0.864. The results demonstrate that the model can reliably explain and predict the differences between the three groups of samples.

4.3.2. Orthogonal partial least squares discriminant analysis (OPLS-DA)

The supervised identification and multivariate statistical analysis technique, Orthogonal Partial Least Squares Discriminant Analysis (OPLS-DA), was employed to establish correlation models between the expression of metabolites and individual samples in each group. OPLS-DA can eliminate interference from factors unrelated to the classification information, thus improving the analytical and effective capabilities of the model. As shown in Fig. 4, the R^2X value between the normal control group and the model group is 0.667, R^2Y is 0.991, and Q^2 is 0.864. These values indicate that the X and Y variables explain 66.7 % and 99.1 % of the model's variation, respectively. If new data were to be included to construct the model, the predictability of the model for grouping accuracy would reach 86.4 %. The R^2X value between the model group and the graphene nuangong acupoint plaster group is 0.588, R^2Y is 0.999, and Q^2 is 0.579. These results suggest that the constructed model is reliable.

4.3.3. Significantly different metabolites

The OPLS-DA model was utilized to analyze metabolites with significant differences between groups. The criteria for determining differentially expressed metabolites were set as having a Variable Importance for the Projection (VIP) value greater than 1 and a p-value less than 0.05 based on one-way analysis of variance (ANOVA).

According to the aforementioned screening criteria, a total of 79 differentially expressed metabolites were identified between the model group and the normal group. Among them, 40 metabolites were identified in the positive ion mode, while 39 were identified in the negative ion mode. Among the 23 enriched metabolic pathways significantly associated with the model group compared to the
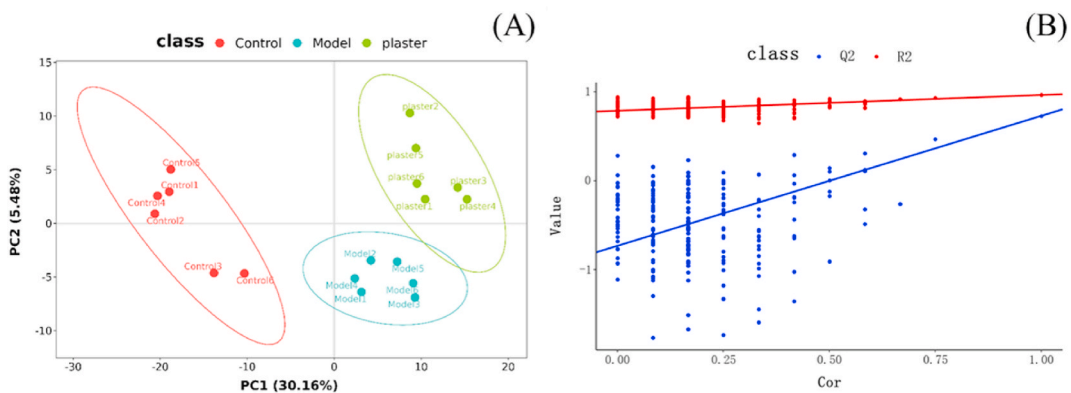

Fig. 3. (A): the PLS-DA scatter plot of the normal control group, model group, and graphene nuangong acupoint plaster group in total ion mode is displayed; (B): the permutation test of the PLS-DA model for the normal control group, model group, and graphene nuangong acupoint plaster group in total ion mode is shown.
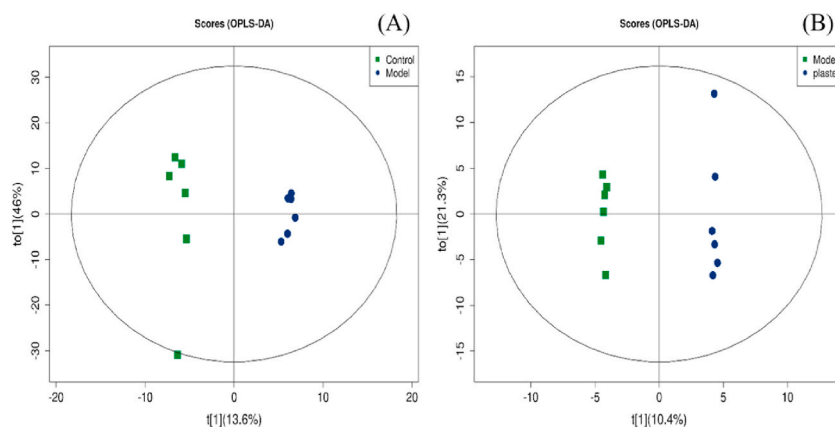
Fig. 4. (A): Plot of OPLS-DA scores for the normal control group and the model group; (B): Plot of OPLS-DA scores for the model group and the graphene nuangong acupoint plaster.

normal group, there were 27 differentially expressed metabolites, as shown in Table 1. Hierarchical super class classification revealed that the differentially expressed metabolites were mainly concentrated in lipid and lipophilic molecules, organic acids and their derivatives, and organic oxygen compounds. Metabolites such as maltotriose, Uridine 5′-monophosphate, taurocholate, 4-aminobutyric acid and pyruvate, and phosphocholine were significantly up-regulated in the model group, and metabolites such as 20-hydroxyarachidonic acid, pregnenolone, 2-aminoadipic acid, thymine, and glycine were significantly down-regulated.

In comparison between the graphene nuangong acupoint plaster group and the model group, a total of 9 significantly different metabolites were identified, with 2 in the positive ion mode and 7 in the negative ion mode. Among these, 3 metabolites were downregulated, while 6 metabolites were upregulated. The details are shown in Table 2.

4.3.4. Metabolic pathway analysis

The metabolic pathways associated with Parkinson's disease (PD) were analyzed using the KEGG database (Kyoto Encyclopedia of Genes and Genomes, http://www.kegg.jp/) and the MetaboAnalyst 4.0 platform. Fisher's Exact Test was employed to screen for significantly enriched metabolic pathways ($P < 0.05$) or pathways with an impact factor >0. The biological processes of key pathways were further analyzed. In the comparison between the model group and the normal group, 23 significantly enriched metabolic pathways were identified, as shown in Table 3. Among them, there were 10 pathways that showed highly significant correlations ($P < 0.01$), including amino acid metabolism, arachidonic acid metabolism, and pyrimidine metabolism. Additionally, there were 13 pathways that showed significant correlations ($P < 0.05$), including ovarian steroidogenesis, arginine biosynthesis, and niacin and nicotinamide metabolism. Within the arachidonic acid metabolism pathway, three types of differentially expressed metabolites were found, including prostaglandin D2, 20-hydroxyeicosatetraenoic acid, and phospholipids. Within the ovarian steroidogenesis pathway, pregnenolone ketone was significantly upregulated, indicating its involvement in progesterone synthesis.

The differential metabolites between the graphene nuangong acupoint plaster group and the model group were subjected to pathway analysis, revealing 9 metabolic pathways, as shown in Table 4. Among them, Vitamin B6 metabolism showed a significant correlation ($P < 0.05$). Other pathways such as Ascorbate and aldarate metabolism, Tyrosine metabolism, and Nicotinate and nicotinamide metabolism may be considered as potentially correlated metabolic pathways ($P > 0.05$).

5. Discussion

Graphene and its derivatives possess excellent antibacterial properties, drug-loading capabilities, biocompatibility, and low toxicity, making them widely utilized in the field of biomedicine [10,11]. Additionally, polymer hydrogels exhibit favorable characteristics such as antimicrobial activity, conductivity, antioxidant properties, and adhesion. They are commonly used as clinical dressings to promote wound healing and enhance transdermal drug permeation [12,13]. Graphene Nuangong Acupoint Plaster combine traditional herbal formulations with materials like graphene and hydrogels as drug carriers. These patches aim to address the limitations of traditional topical therapy, including short onset time, skin sensitivity, and low transdermal drug delivery rate, providing a new approach for the treatment of PD.

The prescription of Graphene Nuangong Acupoint Plaster includes Corydalis yanhusuo, cloves, cinnamon, dried ginger, Sinapis semen, Cistanche deserticola, fennel, Sichuan pepper, mugwort leaf, Cyperus rotundus, and Evodia rutaecarpa. These herbs are mixed in equal proportions with 1 ‰ graphene powder. The main active component of Corydalis yanhusuo, tetrahydropalmatine (THP), is a natural alkaloid that has been used to treat various types of pain and inflammatory diseases [14]. Researchers have found that the major chemical constituents of Corydalis yanhusuo can exert analgesic effects by inhibiting glial cell activation and inducing apoptosis, as well as exhibiting anti-inflammatory effects by reducing endogenous inflammatory factor levels [15,16]. Euodiae Fructus contains multiple pharmacologically active components with anti-inflammatory, analgesic, and antimicrobial properties. It can also regulate levels of PGE_2, ET-1, P2X3, and Ca^{2+} in the uterine smooth muscle of rats with dysmenorrhea, improving the tension state of the

Table 1
Potential differential metabolites in primary dysmenorrhea model rats.

Name	Fold. change	*p*-value	VIP	*m/z*	rt(s)	adduct	Trend	ESI	SuperClass
Maltotriose	11.112	0.000	11.444	503.161	451.759	[M-H]-	↑	–	Organic oxygen compounds
Uridine 5′-monophosphate	8.928	0.000	5.758	325.113	439.185	[M+H]+	↑	+	Nucleosides, nucleotides, and analogues
Taurocholate	6.703	0.006	2.767	514.283	199.036	[M-H]-	↑	–	Lipids and lipid-like molecules
Isomaltose	4.651	0.000	7.824	341.108	391.152	[M-H]-	↑	–	Organic oxygen compounds
Trehalose	4.585	0.000	9.641	360.150	371.668	[M+NH4]+	↑	+	Organic oxygen compounds
D-Maltose	4.009	0.000	3.354	401.129	390.981	(M+CH3COO)-	↑	–	Organooxygen compounds
Maltose	3.701	0.000	6.688	365.105	371.395	[M+Na]+	↑	+	Organic oxygen compounds
4-Aminobutyric acid(GABA)	3.630	0.000	3.025	104.070	349.747	[M+H]+	↑	+	Organic acids and derivatives
Cellobiose	3.458	0.000	1.762	381.079	372.113	(M+K)+	↑	+	Organic oxygen compounds
Taurochenodeoxycholate	2.968	0.006	2.224	498.288	157.559	[M-H]-	↑	–	Lipids and lipid-like molecules
Pyruvate	2.822	0.005	6.750	87.009	123.461	[M-H]-	↑	–	Organic acids and derivatives
1-(3-pyridyl)-1-butanone-4-carboxylic acid	2.471	0.001	1.710	134.080	58.694	[M+H-CH2O2]+	↑	+	Organic acids and derivatives
Phosphocholine	2.085	0.007	5.565	367.139	473.072	[2 M+H]+	↑	+	Organic nitrogen compounds
2′-Deoxycytidine 5′-monophosphate (dCMP)	1.941	0.002	1.023	323.077	478.738	(M+NH4-2H)-	↑	–	Nucleosides, nucleotides, and analogues
L-citrulline	1.760	0.002	1.338	174.088	390.498	[M-H]-	↑	–	Organic acids and derivatives
Fructose 1,6-diphosphate	1.572	0.032	1.346	338.988	501.130	[M-H]-	↑	–	Organic oxygen compounds
Argininosuccinic acid	1.540	0.006	1.523	291.129	459.852	[M+H]+	↑	+	Organic acids and derivatives
PGD2	0.664	0.025	2.069	351.217	116.173	[M-H]-	↓	–	Lipids and lipid-like molecules
L-Tyrosine	0.663	0.041	1.360	182.080	314.955	(M+H)+	↓	+	Organic acids and derivatives
PC(16:0/16:0)	0.661	0.006	4.453	734.568	69.473	[M+H]+	↓	+	Lipids and lipid-like molecules
Thymidine 5′-monophosphate	0.646	0.032	1.202	321.039	69.341	[M-H]-	↓	–	Nucleosides, nucleotides, and analogues
Glycine	0.586	0.008	2.550	74.024	363.125	(M-H)-	↓	–	Organic acids and derivatives
Thymine	0.509	0.002	2.236	125.035	73.809	[M-H]-	↓	–	Organoheterocyclic compounds
2-aminoadipic acid	0.440	0.010	1.142	162.075	392.364	[M+H]+	↓	+	Organic acids and derivatives
12s-hydroxy-5z,8z,10e,14z-eicosatetraenoic acid	0.304	0.004	9.154	319.227	37.168	[M-H]-	↓	–	Lipids and lipid-like molecules
Pregnenolone	0.261	0.032	1.506	317.246	32.161	[M+H]+	↓	+	Lipids and lipid-like molecules
20-hydroxyarachidonic acid	0.100	0.002	1.283	639.460	53.511	[2M-H]-	↓	–	Lipids and lipid-like molecules

uterine smooth muscle [17]. Additionally, various extracts of Euodiae Fructus, such as rutaecarpine (Rut), dehydroevodiamine (Deh), and evodianinine (Evo), have been found to possess analgesic and anti-inflammatory effects [18,19]. The main chemical component of cloves is clove volatile oil, which exhibits antioxidant, anti-inflammatory, antibacterial, and analgesic effects, while also promoting transdermal absorption [20,21]. Previous studies have shown that polyphenols in cinnamon can modulate macrophage anti-inflammatory phenotypes, and cinnamaldehyde (CA) can inhibit the expression of pro-inflammatory cytokines [22,23]. Furthermore, the essential oil of Cinnamomum species can reduce the levels of $PGF_{2\alpha}$, Ca^{2+}, and cyclooxygenase-2 (COX-2) in uterine tissues, thereby alleviating uterine smooth muscle spasms in a dysmenorrhea rat model [24]. Fennel contains volatile oils, organic acids, sterols, and other components that have anti-inflammatory, antioxidant, and antibacterial effects. They can reduce the intensity of uterine contractions induced by oxytocin and PGE2 in dysmenorrhea rats [25,26]. Researchers have found that Cistanche deserticola extracts can improve oxidative stress, DNA damage, cell apoptosis, and inflammatory injury [27,28]. Additionally, Sichuan pepper [29,30], mugwort leaf [31,32], and Cyperus rotundus [33] contain volatile oils and their main constituents, which exhibit anti-inflammatory, antioxidant, and analgesic effects. Dried ginger can improve the pathological condition of the uterus in a Parkinson's disease rat model by modulating the ERK1/2/NF-κB signaling pathway mediated by transient receptor potential (TRP) ion channels [34]. In summary, the pharmaceutical ingredients of GNGAP possess analgesic and anti-inflammatory properties, providing assurance for the treatment of PD.

After modeling with combined estradiol and oxytocin, significant changes in prostaglandins were observed in the uteri of model

Table 2
Differential metabolites screened in the graphene nuangong acupoint plaster group vs. model group.

Name	Fold. change	p-value	VIP	m/z	rt(s)	adduct	Trend	ESI	SuperClass
Orotidine	1.638	0.027	2.266	287.051	310.040	[M-H]-	↑	−	Organoheterocyclic compounds
1-Methylnicotinamide	0.621	0.023	3.980	137.070	271.831	M+	↓	+	Organoheterocyclic compounds
4-pyridoxic acid	3.599	0.001	1.909	182.045	43.610	[M-H]-	↑	−	Organoheterocyclic compounds
D-glucarate	1.655	0.037	2.461	208.985	160.184	[M-H]-	↑	−	Organic oxygen compounds
Philanthotoxin 74	2.132	0.013	1.231	433.330	102.457	[M-H]-	↑	−	Organic acids and derivatives
Tetrahydrocorticosterone	2.789	0.004	5.529	349.237	139.971	[M-H]-	↑	−	Lipids and lipid-like molecules
Siduron	0.644	0.031	2.560	137.070	343.349	[M+H-C7H12]+	↓	+	Benzenoids
Phenol	1.760	0.026	2.602	93.0344	26.926	[M-H]-	↑	−	Benzenoids
1-Palmitoyl-2-oleoyl-sn-glycero-3-phosphate	0.261	0.018	2.921	673.480	36.977	(M-H)-	↓	−	NA

Note: NA: Not identified to.

Table 3
Significant enrichment of metabolic pathways in model group vs. normal group.

Map_Name	p. value	richFactor	Related Metabolites
Starch and sucrose metabolism	0.0007	0.1081	D-Maltose, Isomaltose, Cellobiose, Maltose, Trehalose
Central carbon metabolism in cancer	0.0007	0.1081	Fructose 1,6-diphosphate, Glycine, Pyruvate, L-Tyrosine
Biosynthesis of amino acids	0.0029	0.0469	Glycine, L-citrulline, Pyruvate, 2-aminoadipic acid, Argininosuccinic acid, L-Tyrosine
Alanine, aspartate and glutamate metabolism	0.0036	0.1071	Pyruvate, 4-Aminobutyric acid(GABA), Argininosuccinic acid
Thiamine metabolism	0.0049	0.0968	Glycine, Pyruvate, L-Tyrosine
Cholesterol metabolism	0.0053	0.2000	Taurochenodeoxycholate, Taurocholate
Pyrimidine metabolism	0.0059	0.0615	2′-Deoxycytidine 5′-monophosphate (dCMP), Thymidine 5′-monophosphate, Thymine, Uridine 5′-monophosphate
Choline metabolism in cancer	0.0064	0.1818	PC(16:0/16:0), Phosphocholine
Synaptic vesicle cycle	0.0077	0.1667	Glycine, 4-Aminobutyric acid(GABA)
Arachidonic acid metabolism	0.0097	0.0533	12s-hydroxy-5z,8z,10e,14z-eicosatetraenoic acid, 20-hydroxyarachidonic acid, PGD2, PC(16:0/16:0)
Primary bile acid biosynthesis	0.0155	0.0638	Glycine, Taurochenodeoxycholate, Taurocholate
ABC transporters	0.0182	0.0365	D-Maltose, Glycine, Maltotriose, Cellobiose, Maltose, Trehalose
Retrograde endocannabinoid signaling	0.0189	0.1053	4-Aminobutyric acid(GABA), PC(16:0/16:0)
Neuroactive ligand-receptor interaction	0.0203	0.0577	Glycine, PGD2, 4-Aminobutyric acid(GABA)
Nicotinate and nicotinamide metabolism	0.0235	0.0545	Pyruvate, 1-(3-pyridyl)-1-butanone-4-carboxylic acid, 4-Aminobutyric acid(GABA)
Aldosterone synthesis and secretion	0.0250	0.0909	12s-hydroxy-5z,8z,10e,14z-eicosatetraenoic acid, Pregnenolone
AMPK signaling pathway	0.0250	0.0909	Fructose 1,6-diphosphate, Pyruvate
Taurine and hypotaurine metabolism	0.0250	0.0909	Pyruvate, Taurocholate
Arginine biosynthesis	0.0272	0.0870	L-citrulline, Argininosuccinic acid
Ovarian steroidogenesis	0.0294	0.0833	12s-hydroxy-5z,8z,10e,14z-eicosatetraenoic acid, Pregnenolone
Glucagon signaling pathway	0.0342	0.0769	Fructose 1,6-diphosphate, Pyruvate
Carbohydrate digestion and absorption	0.0367	0.0741	D-Maltose, Maltotriose, Maltose
Taste transduction	0.0500	0.0625	D-Maltose, 4-Aminobutyric acid(GABA), Maltose

rats, along with torsion responses and a significant increase in uterine organ coefficient, indicating successful modeling in this study. The metabolism of arachidonic acid plays an important role in the occurrence and development of inflammatory reactions. Arachidonic acid and its metabolites, such as prostaglandins and leukotrienes, directly regulate inflammatory factors in the body [35,36]. Fang Hong et al. [37] found that differential metabolites in the serum of PD model rats were mainly enriched in biological metabolic pathways such as arachidonic acid, unsaturated fatty acids, nitrite, and amino acids. In this study, compared to the normal group, differential metabolites in the uterus of the model group rats were significantly enriched in the AA metabolic pathway, and significant changes were observed in PGD_2, 20-HETE, lecithin, and 12(S)-HETE in this pathway. Li Na et al. [38] discovered 31 differential metabolites in the serum of PD model rats, including cholesterol, L-tyrosine, and citric acid, which are mainly involved in primary bile acid synthesis, various amino acid and glycerophospholipid biosynthesis in the body. Lama Assaf et al. [39] suggested that the mTOR/AMPK signaling pathway promotes uterine cell growth, migration, and proliferation through the regulation of steroids and

Table 4

Enrichment of KEGG pathway in uterine tissue samples of graphene nuangong acupoint plaster group vs. model group.

Map_Name	p.value	richFactor	Related Metabolites
Vitamin B6 metabolism	0.0462	0.0357	4-pyridoxic acid
Protein digestion and absorption	0.0765	0.0213	Phenol
Ascorbate and aldarate metabolism	0.0797	0.0204	D-glucarate
Nicotinate and nicotinamide metabolism	0.0890	0.0182	1-Methylnicotinamide
Pyrimidine metabolism	0.1045	0.0154	Orotidine
Tyrosine metabolism	0.1242	0.0128	Phenol
Bile secretion	0.1523	0.0103	1-Methylnicotinamide
Steroid hormone biosynthesis	0.1553	0.0101	Tetrahydrocorticosterone
Metabolic pathways	0.5655	0.0018	4-pyridoxic acid, D-glucarate, Orotidine, Phenol, 1-Methylnicotinamide

other hormones, thereby improving uterine inflammation and oxidative stress response. In this study, 79 differential metabolites were screened in the uterine tissues of the model group compared to the blank group, mainly enriched in 23 significantly metabolic pathways, including primary bile acid biosynthesis, AMPK signaling pathway, and ovarian steroidogenesis. Among these 23 metabolic pathways, 27 relevant differential metabolites were identified. These findings are consistent with previous studies while also identifying potential biomarkers for PD occurrence.

The results of this study showed that GNGAP significantly regulated the levels of $PGF_{2\alpha}$ and PGE_2 in the uteri of PD model rats, thereby reducing the number of torsion responses and the uterine organ coefficient in the model rats. Metabolomic analysis revealed that compared to the model group, 9 differential metabolites were identified in the uteri of the graphene nuangong acupoint plaster group rats, including 4-pyridoxic acid, D-glucarate, orotidine, tetrahydrocorticosterone, phenol, 1-methylnicotinamide, philanthotoxin 74, siduron, and 1-palmitoyl-2-oleoyl-sn-glycero-3-phosphate. 4-Pyridoxic acid is a degradation product of vitamin B6, and it was significantly upregulated in the uteri of the graphene nuangong acupoint plaster group rats compared to the model group, with significant enrichment in the Vitamin B6 metabolism pathway. B-complex vitamins can regulate inflammation and neurotransmitter levels in neuropathic pain, and they possess anti-inflammatory, antioxidant, and nerve repair functions [40]. Per Magne Ueland et al. [41] suggested that vitamin B6, as a co-factor, participates in immune regulation and related metabolic pathways at the local site of inflammation. Further research has shown that vitamin B6 not only inhibits the NF-κB and MAPK signaling pathways but also regulates the activity of sphingosine-1-phosphate lyase (SPL) in macrophages, reducing the level of sphingosine-1-phosphate (S1P) and exerting anti-inflammatory effects [42]. D-glucarate is one of the glucose derivatives found in fruits and vegetables and can also be secreted in small amounts in mammalian bodies. Compared to the model group, there was a significant increase in D-glucarate in the uteri of the graphene nuangong acupoint plaster group rats. Studies have shown that metabolites derived from the oxidation of D-glucarate can participate in body metabolism, lower estrogen levels, regulate hormone environments, and possess antioxidant properties [43,44]. In addition, there was a significant increase in phenol in the uteri of the graphene nuangong acupoint plaster group rats compared to the model group. Researchers have found that phenolic compounds in blood-activating and stasis-resolving herbal medicines can alleviate the contraction of uterine smooth muscle in PD model rats, thereby providing analgesic effects [45]. 1-Methylnicotinamide is a direct metabolite of niacin and has various immune-regulatory properties, and it can inhibit the activation of the NLRP3 inflammasome by regulating reactive oxygen species levels [46]. Moreover, niacin is catalyzed by nicotinamide N-methyltransferase to generate 1-Methylnicotinamide, and overexpression of nicotinamide N-methyltransferase can activate the STAT3/IL1β/PGE2 pathway, leading to worsened inflammatory reactions [47]. Compared to the model group rats, there was a significant decrease in 1-Methylnicotinamide in the uteri of the graphene nuangong acupoint plaster group rats.

In addition to the pharmacological effects, graphene nuangong acupoint plaster also includes the stimulation of acupoints. In this study, we selected Guanyuan (CV4), Sanyinjiao (SP6), and Zigong (EX-CA1) as the application sites. Guanyuan, Zigong, and Sanyinjiao are commonly used for the treatment of PD [48,49], with Sanyinjiao having an immediate analgesic effect and causing changes in cerebral blood flow (CBF) in specific brain regions [50]. The graphene nuangong acupoint plaster exerts intervention effects through the combination of drug formulation and acupoint stimulation, regulating prostaglandin levels in the uteri of rats with primary dysmenorrhea, reducing twisting responses and uterine organ coefficients, and affecting the expression of uterine metabolites and related metabolic pathways. However, further research is still needed.

This study found that the induction of PD in rats with benzoic acid estradiol combined with oxytocin resulted in uterine metabolic disorders, affecting 23 metabolic pathways including amino acid metabolism, arachidonic acid metabolism, ovarian steroidogenesis, and nicotinate and nicotinamide metabolism. Graphene Nuangong Acupoint Plaster were able to regulate uterine metabolites in primary dysmenorrhea rats, reducing torsion responses and uterine coefficients by intervening in metabolic processes such as Vitamin B6 metabolism, protein digestion and absorption, and nicotinate and nicotinamide metabolism. This study is the first to use uterine metabolomics to reveal the biological mechanism of GNGAP in treating PD and further explore the potential pathogenesis of PD, providing new insights and strategies for the diagnosis and treatment of this disease.

Ethics and dissemination

The research protocol has been reviewed and approved by the Animal Care and Welfare Committee of Changchun University of Chinese Medicine, with approval number: 2022005.

Data availability statement

Data will be made available on request.

CRediT authorship contribution statement

Wu Liu: Writing – original draft, Software, Methodology, Investigation, Formal analysis, Data curation, Conceptualization. **Ting Zhang:** Methodology, Data curation. **Zhaoduan Hu:** Supervision, Project administration. **Xin Li:** Visualization, Investigation. **Fuchun Wang:** Writing – review & editing, Supervision, Resources, Funding acquisition, Conceptualization. **Rui Peng:** Writing – review & editing, Supervision.

Declaration of competing interest

The authors declare that they have no known competing financial interests or personal relationships that could have appeared to influence the work reported in this paper.

Appendix A. Supplementary data

Supplementary data to this article can be found online at https://doi.org/10.1016/j.heliyon.2024.e25268.

References

[1] ACOG committee opinion No. 760: dysmenorrhea and endometriosis in the adolescent, Obstet. Gynecol. 132 (6) (2018) e249–e258, https://doi.org/10.1097/AOG.0000000000002978.
[2] E. Ferries-Rowe, E. Corey, J.S. Archer, Primary dysmenorrhea: diagnosis and therapy, Obstet. Gynecol. 136 (5) (2020) 1047–1058, https://doi.org/10.1097/AOG.0000000000004096.
[3] K.A. Kho, J.K. Shields, Diagnosis and management of primary dysmenorrhea, JAMA 323 (3) (2020) 268–269, https://doi.org/10.1001/jama.2019.16921.
[4] F.A. Oladosu, F.F. Tu, K.M. Hellman, Nonsteroidal antiinflammatory drug resistance in dysmenorrhea: epidemiology, causes, and treatment, Am. J. Obstet. Gynecol. 218 (4) (2018) 390–400, https://doi.org/10.1016/j.ajog.2017.08.108.
[5] M.Y. Zhao, P. Zhang, J. Li, et al., Influence of de qi on the immediate analgesic effect of SP6 acupuncture in patients with primary dysmenorrhoea and cold and dampness stagnation: a multicentre randomised controlled trial, Acupunct. Med. 35 (5) (2017) 332–338, https://doi.org/10.1136/acupmed-2016-011228.
[6] S. Iacovides, I. Avidon, F.C. Baker, What we know about primary dysmenorrhea today: a critical review, Hum. Reprod. Update 21 (6) (2015) 762–778, https://doi.org/10.1093/humupd/dmv039.
[7] J. Liang, M.Y. Han, Z. Luo, et al., Network meta-analysis of 8 acupuncture treatments for primary dysmenorrhoea, Moderniz. Trad. Chinese Med. Materia Medica-World Sci. Technol. 23 (12) (2021) 4593–4605.
[8] Y. Wang, L. Yang, X. Zhang, et al., Quality marker discovery of Danggui Jianzhong decoction for treating primary dysmenorrhoea based on chinmedomics strategy, Phytomedicine 115 (2023) 154724, https://doi.org/10.1016/j.phymed.2023.154724.
[9] N.L.M. Quintão, J.P. Reis, L. Benvenutti, et al., Involvement of a neutrophil-mast cell axis in the effects of Piper malacophyllum (C. PESL) C. DC extract and its isolated compounds in a mouse model of dysmenorrhoea, Inflammopharmacology 30 (6) (2022) 2489–2504, https://doi.org/10.1007/s10787-022-01032-9.
[10] A.I. Lazăr, K. Aghasoleimani, A. Semertsidou, et al., Graphene-related nanomaterials for biomedical applications, Nanomaterials 13 (6) (2023) 1092, https://doi.org/10.3390/nano13061092. Published 2023 Mar 17.
[11] J. Lu, A. Zhang, F. Zhang, et al., Ganoderenic acid D-loaded functionalized graphene oxide-based carrier for active targeting therapy of cervical carcinoma, Biomed. Pharmacother. 164 (2023) 114947, https://doi.org/10.1016/j.biopha.2023.114947.
[12] L. Qiao, Y. Liang, J. Chen, et al., Antibacterial conductive self-healing hydrogel wound dressing with dual dynamic bonds promotes infected wound healing, Bioact. Mater. 30 (2023) 129–141, https://doi.org/10.1016/j.bioactmat.2023.07.015.
[13] S. Xiong, S. Ye, P. Ni, et al., Polyvinyl-alcohol, chitosan and graphene-oxide composed conductive hydrogel for electrically controlled fluorescein sodium transdermal release, Carbohydr. Polym. 319 (2023) 121172, https://doi.org/10.1016/j.carbpol.2023.121172.
[14] Q. Du, X. Meng, S. Wang, A comprehensive review on the chemical properties, plant sources, pharmacological activities, pharmacokinetic and toxicological characteristics of tetrahydropalmatine, Front. Pharmacol. 13 (2022) 890078, https://doi.org/10.3389/fphar.2022.890078. Published 2022 Apr 26.
[15] B. Liu, M. Luo, D. Meng, et al., Tetrahydropalmatine exerts analgesic effects by promoting apoptosis and inhibiting the activation of glial cells in rats with inflammatory pain, Mol. Pain 17 (2021) 17448069211042117, https://doi.org/10.1177/17448069211042117.
[16] G.Y. Xia, D.J. Fang, L.Y. Wang, et al., 13,13a-seco-protoberberines from the tubers of Corydalis yanhusuo and their anti-inflammatory activity, Phytochemistry 194 (2022) 113023, https://doi.org/10.1016/j.phytochem.2021.113023.
[17] Y. Liu, H. Li, L. Chen, et al., Mechanism and pharmacodynamic substance basis of raw and wine-processed Evodia rutaecarpa on smooth muscle cells of dysmenorrhea mice, Pain Res. Manag. 2023 (2023) 7711988, https://doi.org/10.1155/2023/7711988.
[18] W.D. Zhang, X.Y. Chen, C. Wu, et al., Evodiamine reduced peripheral hypersensitivity on the mouse with nerve injury or inflammation, Mol. Pain 16 (2020 Jan-Dec) 1744806920902563, https://doi.org/10.1177/1744806920902563.
[19] S. Fu, L. Liao, Y. Yang, et al., The pharmacokinetics profiles, pharmacological properties, and toxicological risks of dehydroevodiamine: a review, Front. Pharmacol. 13 (2022 Nov 18) 1040154, https://doi.org/10.3389/fphar.2022.1040154.
[20] P. Wang, Z.Z. Wang, Y.M. Liu, et al., Progress on the chemical composition and pharmacological effects of the volatile oil of clove, Chin. Tradit. Pat. Med. 44 (3) (2022) 871–878.
[21] J.N. Haro-González, G.A. Castillo-Herrera, M. Martínez-Velázquez, et al., Clove essential oil (Syzygium aromaticum L. Myrtaceae): extraction, chemical composition, food applications, and essential bioactivity for human health, Molecules 26 (21) (2021) 6387, https://doi.org/10.3390/molecules26216387. Published 2021 Oct 22.

[22] L.K. Chao, K.F. Hua, H.Y. Hsu, et al., Cinnamaldehyde inhibits pro-inflammatory cytokines secretion from monocytes/macrophages through suppression of intracellular signaling, Food Chem. Toxicol. 46 (1) (2008) 220–231, https://doi.org/10.1016/j.fct.2007.07.016.

[23] Y. Song, Y.S. Jung, S. Park, et al., Anti-inflammatory effects and macrophage activation induced by bioavailable cinnamon polyphenols in mice [published online ahead of print, 2023 Sep 1], Mol. Nutr. Food Res. (2023) e2200768, https://doi.org/10.1002/mnfr.202200768.

[24] L. Sun, L.N. Liu, J.C. Li, et al., The essential oil from the twigs of Cinnamomum cassia Presl inhibits oxytocin-induced uterine contraction in vitro and in vivo, J. Ethnopharmacol. 206 (2017) 107–114, https://doi.org/10.1016/j.jep.2017.05.023.

[25] F. Rafieian, R. Amani, A. Rezaei, et al., Exploring fennel (Foeniculum vulgare): composition, functional properties, potential health benefits, and safety, Crit. Rev. Food Sci. Nutr. (2023) 1–18, https://doi.org/10.1080/10408398.2023.2176817.

[26] S.N. Ostad, M. Soodi, M. Shariffzadeh, et al., The effect of fennel essential oil on uterine contraction as a model for dysmenorrhea, pharmacology and toxicology study, J. Ethnopharmacol. 76 (3) (2001) 299–304, https://doi.org/10.1016/s0378-8741(01)00249-5.

[27] D. Zhang, C. Lu, Z. Yu, et al., Echinacoside alleviates UVB irradiation-mediated skin damage via inhibition of oxidative stress, DNA damage, and apoptosis, Oxid. Med. Cell. Longev. 2017 (2017) 6851464, https://doi.org/10.1155/2017/6851464.

[28] H. Zhang, Z. Xiang, X. Duan, et al., Antitumor and anti-inflammatory effects of oligosaccharides from Cistanche deserticola extract on spinal cord injury, Int. J. Biol. Macromol. 124 (2019) 360–367, https://doi.org/10.1016/j.ijbiomac.2018.11.132.

[29] H. Zhang, Z. Guo, X. Wang, et al., Protective mechanisms of Zanthoxylum bungeanum essential oil on DSS-induced ulcerative colitis in mice based on a colonic mucosal transcriptomic approach [published correction appears in Food Funct. 2023 Feb 6;14(3):1795], Food Funct. 13 (18) (2022) 9324–9339, https://doi.org/10.1039/d1fo04323d. Published 2022 Sep. 22.

[30] M. Zhang, J. Wang, L. Zhu, et al., Zanthoxylum bungeanum Maxim. (Rutaceae): a systematic review of its traditional uses, botany, phytochemistry, pharmacology, pharmacokinetics, and toxicology, Int. J. Mol. Sci. 18 (10) (2017) 2172, https://doi.org/10.3390/ijms18102172. Published 2017 Oct 18.

[31] S.M. Kim, S.J. Lee, V. Venkatarame Gowda Saralamma, et al., Polyphenol mixture of a native Korean variety of Artemisia argyi H. (Seomae mugwort) and its anti-inflammatory effects, Int. J. Mol. Med. 44 (5) (2019) 1741–1752, https://doi.org/10.3892/ijmm.2019.4334.

[32] Q. Hu, Z. Liu, Y. Guo, S. Lu, H. Du, Y. Cao, Antioxidant capacity of flavonoids from Folium Artemisiae Argyi and the molecular mechanism in Caenorhabditis elegans, J. Ethnopharmacol. 279 (2021) 114398, https://doi.org/10.1016/j.jep.2021.114398.

[33] F. Wang, S. Zhang, J. Zhang, F. Yuan, Systematic review of ethnomedicine, phytochemistry, and pharmacology of Cyperi Rhizoma, Front. Pharmacol. 13 (2022) 965902, https://doi.org/10.3389/fphar.2022.965902. Published 2022 Oct 7.

[34] X. Liu, X. Meng, X. Su, et al., The mechanism of ginger and its processed products in the treatment of estradiol valerate coupled with oxytocin-induced dysmenorrhea in mice via regulating the TRP ion channel-mediated ERK1/2/NF-κB signaling pathway, Food Funct. 13 (21) (2022) 11236–11248, https://doi.org/10.1039/d2fo01845d. Published 2022 Oct 31.

[35] U.N. Das, Essential fatty acids and their metabolites in the pathobiology of inflammation and its resolution, Biomolecules 11 (12) (2021) 1873, https://doi.org/10.3390/biom11121873. Published 2021 Dec 14.

[36] B. Kaur, P. Singh, Inflammation: biochemistry, cellular targets, anti-inflammatory agents and challenges with special emphasis on cyclooxygenase-2, Bioorg. Chem. 121 (2022) 105663, https://doi.org/10.1016/j.bioorg.2022.105663.

[37] F. Hong, G. He, M. Zhang, et al., The establishment of a mouse model of recurrent primary dysmenorrhea, Int. J. Mol. Sci. 23 (11) (2022) 6128, https://doi.org/10.3390/ijms23116128. Published 2022 May 30.

[38] N. Li, X. Cui, C. Ma, et al., Uncovering the effects and mechanism of danggui shaoyao san intervention on primary dysmenorrhea by serum metabolomics approach, J. Chromatogr., B: Anal. Technol. Biomed. Life Sci. 1209 (2022) 123434, https://doi.org/10.1016/j.jchromb.2022.123434.

[39] L. Assaf, A.A. Eid, J. Nassif, Role of AMPK/mTOR, mitochondria, and ROS in the pathogenesis of endometriosis, Life Sci. 306 (2022) 120805, https://doi.org/10.1016/j.lfs.2022.120805.

[40] A.M. Paez-Hurtado, C.A. Calderon-Ospina, M.O. Nava-Mesa, Mechanisms of action of vitamin B1 (thiamine), B6 (pyridoxine), and B12 (cobalamin) in pain: a narrative review, Nutr. Neurosci. 26 (3) (2023) 235–253, https://doi.org/10.1080/1028415X.2022.2034242.

[41] P.M. Ueland, A. McCann, Midttun Ø, A. Ulvik, Inflammation, vitamin B6 and related pathways, Mol. Aspect. Med. 53 (2017) 10–27, https://doi.org/10.1016/j.mam.2016.08.001.

[42] X. Du, Y. Yang, X. Zhan, et al., Vitamin B6 prevents excessive inflammation by reducing accumulation of sphingosine-1-phosphate in a sphingosine-1-phosphate lyase-dependent manner, J. Cell Mol. Med. 24 (22) (2020) 13129–13138, https://doi.org/10.1111/jcmm.15917.

[43] H. Abou-Issa, M. Moeschberger, W. el-Masry, et al., Relative efficacy of glucarate on the initiation and promotion phases of rat mammary carcinogenesis, Anticancer Res. 15 (3) (1995) 805–810.

[44] J. Saluk-Juszczak, A comparative study of antioxidative activity of calcium-D-glucarate, sodium-D-gluconate and D-glucono-1,4-lactone in a human blood platelet model, Platelets 21 (8) (2010) 632–640, https://doi.org/10.3109/09537104.2010.512210.

[45] H. Ni, J. Liu, O. Dai, et al., Chemical composition and uterine smooth muscle relaxant activity of essential oils from 10 kinds of blood-activating and stasis-resolving Chinese medicinal herbs, J. Ethnopharmacol. 269 (2021) 113713, https://doi.org/10.1016/j.jep.2020.113713.

[46] K. Sidor, A. Jeznach, G. Hoser, T. Skirecki, 1-Methylnicotinamide (1-MNA) inhibits the activation of the NLRP3 inflammasome in human macrophages, Int. Immunopharm. 121 (2023) 110445, https://doi.org/10.1016/j.intimp.2023.110445.

[47] C. Yang, T. Wang, S. Zhu, et al., Nicotinamide N-methyltransferase remodeled cell metabolism and aggravated proinflammatory responses by activating STAT3/IL1β/PGE2 pathway, ACS Omega 7 (42) (2022) 37509–37519, https://doi.org/10.1021/acsomega.2c04286. Published 2022 Oct 12.

[48] W. Cheng, L. Zhang, B. Chen, et al., A study on the regularity of acupoint match based on association rules with SP6 as the main acupoint and its clinical application, Int. J. Gen. Med. 16 (2023) 5675–5693, https://doi.org/10.2147/IJGM.S441978. Published 2023 Dec 4.

[49] S. Yu, Y. Wen, W. Xia, et al., Acupoint herbal plaster for patients with primary dysmenorrhea: study protocol for a randomized controlled trial, Trials 19 (1) (2018) 348, https://doi.org/10.1186/s13063-018-2682-8. Published 2018 Jul 3.

[50] S.L. Peng, H.C. Yang, Y.C. Lee, C.M. Chen, Y.Y. Chen, C.H. Tu, Analgesia effect of verum and sham acupuncture treatments in primary dysmenorrhea: a MRI pilot study, J. Personalized Med. 11 (12) (2021) 1244, https://doi.org/10.3390/jpm11121244. Published 2021 Nov 23.